3-2012

Preconditioning visco-resistive MHD for tokamak plasmas

Daniel R. Reynolds
Southern Methodist University, reynolds@smu.edu

Ravi Samtaney
KAUST

Hilari C. Tiedeman
Southern Methodist University, htiedeman@mail.smu.edu

Preconditioning visco-resistive MHD for tokamak plasmas

Daniel R. Reynolds[1], Ravi Samtaney[2], Hilari C. Tiedeman[1]

[1]Department of Mathematics, Southern Methodist University
[2]Department of Mechanical Engineering, KAUST

2012 Finite Element Rodeo
Rice University
March 2-3, 2012

[Funding support by DOE, KAUST; computing support by SMU CSC]

Compressible Visco-Resistive Magnetohydrodynamics

We consider the compressible visco-resistive MHD model in a mapped cylindrical geometry for modeling tokamak fusion plasmas,

$$\partial_t \mathbf{U} + \frac{1}{r\mathcal{J}}\left[\partial_\xi(r\tilde{\mathbf{F}}(\mathbf{U})) + \partial_\eta(r\tilde{\mathbf{H}}(\mathbf{U})) + \partial_\varphi(\tilde{\mathbf{G}}(\mathbf{U}))\right] = \mathbf{S}(\mathbf{U}) + \nabla\cdot\tilde{\mathbf{F}}_d(\mathbf{U}),$$

where $\mathbf{U} = (\rho, \rho\mathbf{u}, \mathbf{B}, e)^T$.

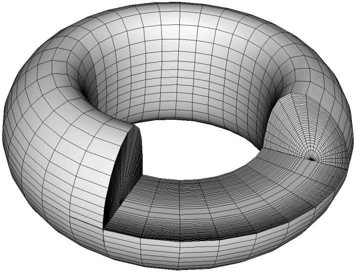

Left: toroidal tokamak domain, with slice removed to show grid structure.

Right: poloidal cross-section.

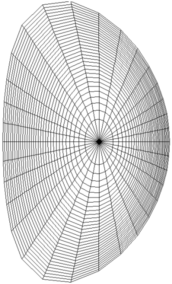

Model Details

The hyperbolic fluxes are given by

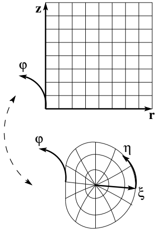

$$\begin{aligned}\tilde{\mathbf{F}} &= \mathcal{J}\left(\partial_r \xi\, \mathbf{F} + \partial_z \xi\, \mathbf{H}\right) &= \partial_\eta z\, \mathbf{F} - \partial_\eta r\, \mathbf{H},\\ \tilde{\mathbf{H}} &= \mathcal{J}\left(\partial_r \eta\, \mathbf{F} + \partial_z \eta\, \mathbf{H}\right) &= \partial_\xi z\, \mathbf{F} - \partial_\xi r\, \mathbf{H},\\ \tilde{\mathbf{G}} &= \mathcal{J}\mathbf{G}.\end{aligned}$$

$\xi = \xi(r,z)$, $\eta = \eta(r,z)$ and $\mathcal{J} = (\partial_\xi r)(\partial_\eta z) - (\partial_\eta r)(\partial_\xi z)$ map between cylindrical and tokamak coordinates. Here,

$$\begin{aligned}\mathbf{F} = \big(&\rho u_r,\ \ \rho u_r^2 + \tilde{p} - B_r^2,\ \ \rho u_r u_\varphi - B_r B_\varphi,\ \ \rho u_r u_z - B_r B_z,\ \ 0,\\ &u_r B_\varphi - u_\varphi B_r,\ \ u_r B_z - u_z B_r,\ \ (e+\tilde{p})u_r - (\mathbf{B}\cdot\mathbf{u})B_r\big)\\ \mathbf{G} = \big(&\rho u_\varphi,\ \ \rho u_r u_\varphi - B_r B_\varphi,\ \ \rho u_\varphi^2 + \tilde{p} - B_\varphi^2,\ \ \rho u_z u_\varphi - B_z B_\varphi,\\ &u_\varphi B_r - u_r B_\varphi,\ 0,\ u_\varphi B_z - u_z B_\varphi,\ (e+\tilde{p})u_\varphi - (\mathbf{B}\cdot\mathbf{u})B_\varphi\big)\\ \mathbf{H} = \big(&\rho u_z,\ \ \rho u_r u_z - B_r B_z,\ \ \rho u_z u_\varphi - B_z B_\varphi,\ \ \rho u_z^2 + \tilde{p} - B_z^2,\\ &u_z B_r - u_r B_z,\ u_z B_\varphi - u_\varphi B_z,\ 0,\ (e+\tilde{p})u_z - (\mathbf{B}\cdot\mathbf{u})B_z\big)\end{aligned}$$

$\tilde{p} = p + \frac{\mathbf{B}\cdot\mathbf{B}}{2}$, $\quad e = \frac{p}{\gamma-1} + \frac{\rho\mathbf{u}\cdot\mathbf{u}}{2} + \frac{\mathbf{B}\cdot\mathbf{B}}{2}$, and $\nabla\cdot\mathbf{F}_d(\mathbf{U})$ adds a small amount of diffusion (viscosity, resistivity, heat conduction).

Space-Time Discretization, Implicit Solver

We discretize in space using a second-order finite volume method, with all unknowns $\mathbf{U}$ located at cell centers.

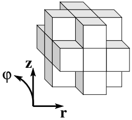

- Tokamak mapping results in a 19 point nearest neighbor stencil in the domain interior.
- Boundaries $\xi = \{\xi_{min}, \xi_{max}\}$, require one-sided stencil.

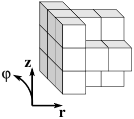

We write the semi-discretized system as $\partial_t \mathbf{U} = \mathcal{R}(\mathbf{U})$, and use an adaptive step/order BDF method in time (CVODE),

$$\mathbf{U}^{n+1} - \beta_0 \Delta t \mathcal{R}(\mathbf{U}^{n+1}) - \sum_{l=0}^{q-1} \left[\alpha_l \mathbf{U}^{n-l} + \beta_l \Delta t \mathcal{R}(\mathbf{U}^{n-l}) \right] = 0.$$

This defines an implicit nonlinear root-finding problem, $\mathbf{f}(\mathbf{U}) = 0$, solved using a matrix-free inexact Newton-BiCGStab solver, with right preconditioning.

Preconditioner Motivation

- Due to strong guide fields, tokamak MHD stiffness primarily arises from fast magnetosonic waves within the poloidal plane.
- While diffusion is present, the coefficients are very small for realistic devices (Reynolds, Lundquist numbers $> 10^7$).
- Strong inter-variable coupling in stiff hyperbolic terms requires a system-level approach (i.e. cannot decouple equations).
- Production tokamak codes (M3D, NIMROD) split the operators geometrically to treat only the poloidal plane implicitly.

Preconditioner Construction

- We consider *restricted additive Schwarz* methods to treat the strong inter-variable coupling in this advection-dominated regime.
- Consider approximations that increase sparsity in preconditioner.
- Strong nonlinearity, geometric complexity and preconditioner flexibility prohibit analytical construction; we use automatic differentiation (OPENAD) to generate preconditioner entries.

Stencil approximations used in constructing P:

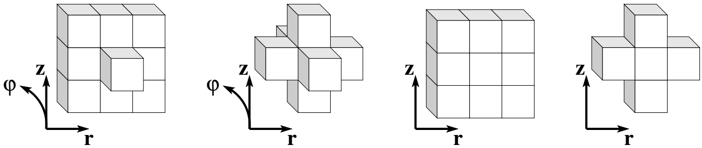

[R. & Samtaney, 2012; R., Samtaney & Tiedeman, 2012]

Restricted Additive Schwarz Preconditioners

RAS [Cai & Sarkis 1999] solves local portions of J separately on each process,

$$P_{RAS} = \sum_i \hat{R}_i^T \tilde{J}_i^{-1} \tilde{R}_i.$$

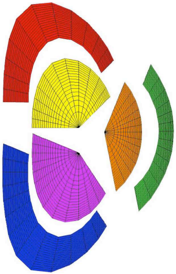

- $\Omega_i \subset \Omega$ is extended to overlap with neighbors, $\tilde{\Omega}_i$.
- $\tilde{R}_i$ restricts $\Omega \to \tilde{\Omega}_i$, $\hat{R}_i^T$ injects $\Omega_i \to \Omega$.
- $\tilde{J}_i^{-1}$ is performed on $\tilde{\Omega}_i$ using SuperLU.

Preconditioners:

* P_{RAS} uses the full 19 point 3D stencil.
* P_{RASp}, P_{RASp5} are poloidal, using the 9 & 5pt stencils.
* We also consider hybrid RAS+ADI approaches,

$$P_{H11} = (I - \gamma J_\varphi)^{-1} P_{RASp}, \qquad \text{[11pt stencil]}$$
$$P_{H7} = (I - \gamma J_\varphi)^{-1} P_{RASp5}. \qquad \text{[7pt stencil]}$$

  φ solved with periodic, parallel, block-tridiagonal solver.
* We allow overlap widths of 2 and 4 cells at each face.

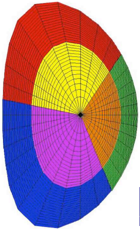

Small-Scale Serial Tests (Lu, $Re = \{10^3, 10^4\}$)

Tested $P = \{I, P_{RAS}, P_{RASp}, P_{RASp5}, P_{H11}, P_{H7}\}$, with overlap 2. Meshes were 16×16×16, 32×32×16, and 64×64×16 ($N_\xi \times N_\eta \times N_\varphi$).

- P_{RAS} only effective on small problems (memory & factorization costs).
- I requires more Krylov, but remains competitive due to simplicity.
- P_{RASp} vs P_{H11} and P_{RASp5} vs P_{H7} are indistinguishable on such small problems.

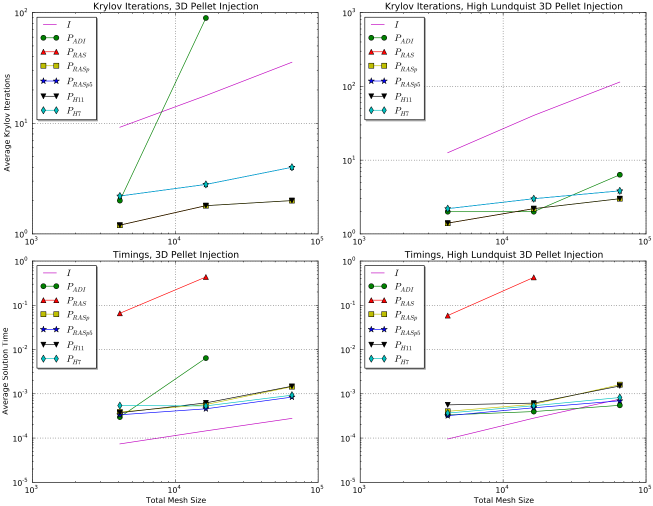

Parallel Tests: $P = \{I, P_{RASp}, P_{RASp5}, P_{H11}, P_{H7}\}$

$Lu = 10^4$ problem: overlaps 2 and 4; weak scaling with $32\times32\times16$ grid/processor.

Questions:

(a) How does RAS overlap width affect P?

(b) How do stencil approximations affect P?

(c) Are toroidal effects important in P?

- I not visible, with $\{16, 18, 36, 34, 44, 96, 106\}$ and $\{32, 40, 102, 108, 120\}$ iterations. Fastest at first, but slows and eventually fails.
- **RAS overlap** (solid vs dashed): more overlap $\Rightarrow$ fewer Krylov, but increased cost per solve dominates.
- **Stencil approximations** ($\circ$ vs Δ, $\square$ vs $\star$): more approx. $\Rightarrow$ more Krylov, but reduced cost per solve dominates.
- **Toroidal P vs 2D** ($\square$ vs $\circ$, $\star$ vs Δ): hybrid $P \Rightarrow$ slightly fewer Krylov, but at slightly increased cost (balances out).

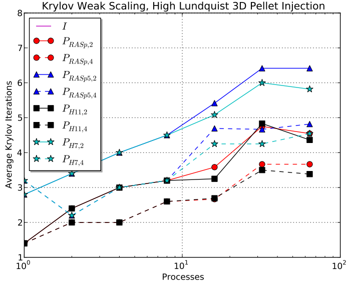

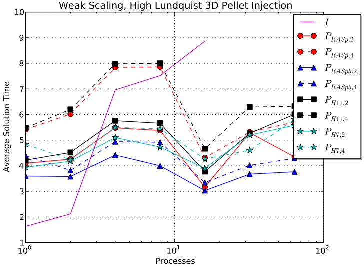

Summary of Current Results

- Extreme flexibility in P thanks to free, high quality, robust AD tools.
- While preconditioning is needed, our most effective approach employed approximations that decreased its cost ($P_{RASp5,2}$):
  - Approximates the 19pt 3D stencil with a simple 5pt 2D version within each poloidal plane,
  - Solves systems using a RAS method with overlap 2.
  - Required the most Krylov iterations per Newton step, but its increased efficiency proved more important.
- Inclusion of φ solve only marginally slowed $P_{H7,2}$, but could increase flexibility when solving problems with additional toroidal effects.

Current & Future Work

Multi-level solver within poloidal planes, for improved scalability with increasing mesh size [with H. Tiedeman].

- 2-level RAS and multi-level Schur complement

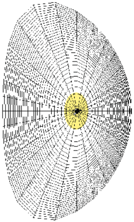

New construction of mapped poloidal mesh to capture geometry while removing x-point [with R. Samtaney & J. Brown].

- Increase stability,
- Sacrifice field-line-following mesh.

ARK-based time integration [with J. Brown & E. Constantinescu]:

- Implicitly follow linearized fast waves and diffusion, explicitly handle slow waves and nonlinearity,
- Accurate/stable coupling between components.

Higher-order solutions, spatial adaptivity (DG?).

- Increased accuracy,
- Concern over $\nabla \cdot \mathbf{B} = 0$ constraint.

Thanks and Acknowledgements

Collaborators:

- Ravi Samtaney, KAUST
- Carol S. Woodward, LLNL

Students:

- Hilari C. Tiedeman, SMU
- David J. Gardner, SMU

Support:

- Frameworks, Algorithms and Scalable Technologies in Mathematics (FASTMath) DOE SciDAC Institute
- Towards Optimal Petascale Simulations (TOPS) DOE SciDAC Center
- SMU Center for Scientific Computation cluster

Software:

- SUNDIALS – http://computation.llnl.gov/casc/sundials
- SuperLU – http://crd.lbl.gov/∼xiaoye/SuperLU

SMU